Genetic algorithm-based optimization for the geometric design of a novel orthopedic implant

Won Suk You[1], Justin Casebier[2], Jacob Mandich[2], and Ravi Balasubramanian[2,*], *Member, IEEE*

***Abstract*—Objective: A tendon-transfer is a reconstructive orthopedic surgery where tendons are re-routed from a non-functioning muscle and attached a functioning muscle. Prior work has shown that using a passive implanted device in the ECRL-to-FDP tendon-transfer surgery significantly improves hand grasping function. However, it is still unclear how hand-function improvement, measured by finger joint range of motion and torque, is dependent on the implant's geometry and location within the tendon network. This paper presents a genetic algorithm that determines the device's optimal geometry and location. Methods: hand biomechanical simulation platform was developed to model hand function and also model the tendon-transfer surgery with and without the implant. Finger kinematics and joint torque were used to develop three unique objective functions to optimize the implant's parameters. Results: The optimized device resulted in an 11X increase in finger kinematics with only a 0.9% decrease in joint torque when compared with the biomechanical function enabled by the current suture-based surgery. Conclusion: Designing implantable devices that modify musculoskeletal function is challenging. Factors like tendon routing and joint kinematics create a complex nonlinear system when considering biomechanical function. A genetic algorithm is an effective tool to tackle these nonlinear landscapes to produce optimized designs. Significance: The state-of-the-art surgical procedure to repair high median-ulnar nerve palsy leads to poor hand function and severely limits the patient's ability to perform activities of daily life. This work provides a method for defining relevant objective functions for hand biomechanical function and then uses those objective functions with genetic algorithms to optimize the geometry of an orthopedic implant across multiple variables. The achieved biomechanical function is significantly better than hand function enabled by current surgical procedure.**

***Index Terms*—Genetic algorithm, Kinematic optimization, Orthopedic implant, Tendon transfer surgery.**

I. Introduction

UPPER-EXTREMITY tendon-transfer surgeries have been used since the 1970s to treat neurological disabilities. For example, conditions such as nerve trauma and stroke disable specific forearm and/or hand muscles and prevent patients from performing activities of daily living [1]–[3]. The tendon-transfer surgeries for such conditions detach tendons from a non-functioning muscle and re-attach them using sutures to a functioning donor muscle to partially restore function.

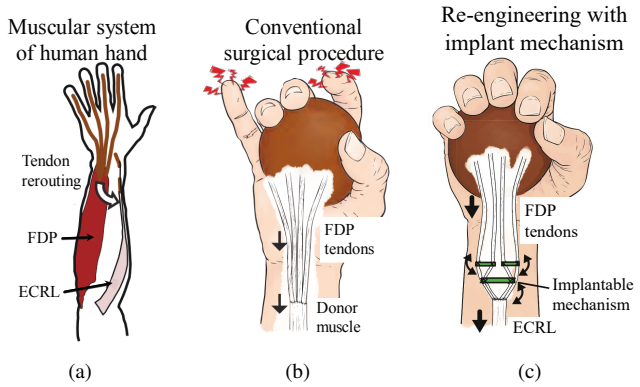

Figure 1: Illustration of the tendon transfer surgery for high median-ulnar nerve palsy including the (a) muscles involved, (b) the conventional tendon transfer surgery, resulting in an incomplete grasp due to coupling, and (c) re-engineering with the proposed implantable mechanism.

While the suture offers a straightforward method for reattaching the tendons, there is a fundamental problem with current surgery—the suture directly couples the input and output tendon(s). In particular, if multiple output tendons are sutured to a single input tendon, the output tendon's movements are equal to the input tendon's movement (see Fig. 1a and b). In such situations, sutures offer little choice when choosing how movement should be transmitted from the input tendon to the output tendons. This limits surgical outcomes.

Our work develops passive implants that when inserted between the output tendons enables the *in situ* surgical construction of "mechanisms", or transmissions that are not 1:1, within the body. The mechanisms will enable re-engineering the transmission of force and movement between the input and the output tendons as per the clinician's recommendation or the patient's requirement. This paper explores the method for optimizing the geometric design of a class of such implants to achieve the desired transmission when one input tendon is sutured to multiple output tendons.

There are at least fifteen tendon-transfer surgeries [4] where multiple output tendons are sutured to a single donor tendon. For example, high median-ulnar nerve palsy disables the flexor digitorum profundus (FDP) muscle. This condition disables finger flexion and prevents patients from conducting fundamental activities like holding a toothbrush or fork. This

This manuscript was submitted on May 11, 2021. This work is supported by the U.S. Department of Defense under grant MR150091 and the U.S. National Science Foundation under grant CBET 1554739.

[1]W. S. You is with Wavemaker Lab, Santa Monica, CA, USA (email: wonsuk87@gmail.com).

[2]All other authors are with the School of Mechanical, Industrial, and Manufacturing Engineering, Oregon State University, Corvallis, OR, USA (correspondence e-mail: casebierjustin@gmail.com).

tendon-transfer surgery re-routes and directly sutures all four FDP tendons to a single wrist extensor muscle. This is typically the extensor carpi radialis longus (ECRL), an expendable wrist extensor (see Fig. 1(a)). The ECRL still functions in this condition, since it is innervated by the radial nerve [5].

Although the standard ECRL-to-FDP tendon-transfer surgery restores adequate finger flexion, the surgery couples the flexion of all four fingers. Thus, if one finger contacts an object during grasping, the other fingers are unable to continue flexing. This is because all four FDP tendons are directly sutured to the ECRL, a muscle with only one muscle compartment. The healthy FDP, in contrast, has four muscle compartments that provide near-independent finger flexion. The fundamental limitation of this surgery is that the fingers cannot adapt to an object's shape during grasping (see Fig. 1(b)). This leads to insecure grasps and significantly limited hand function. Prior work has documented the poor grasp function that arises from the coupled finger movement when multiple tendons are sutured to one muscle [5]–[11]. Specifically, the coupled finger movement leads to (i) incomplete and weak grasps [7], (ii) greater forces required from the muscle to isometrically stretch tendons to flex the other fingers once one finger makes contact, (iii) an uneven stretching of the tendons, which results in even more unbalanced finger movement over time [8], and (iv) large unbalanced forces on the object during the grasping process (observed in robotic hands [12]).

Our group is addressing this problem by developing a passive miniature implant, that when inserted between the finger flexor tendons, creates a "differential mechanism" between the muscle and the fingers. This mechanism enables all fingers to adapt significantly better to an object's shape while grasping even if all four flexor tendons are driven by a single muscle (see Fig. 1(c)). The implantable mechanism's efficacy was confirmed in human hands through initial cadaver experiments [13], [14] and simulation studies [15]. Specifically, these studies showed that the implant enabled the fingers to grasp and conform to an object's shape. In robotic hand design, such differential mechanisms have already been shown to be useful in allowing multiple digits driven by a single actuator to establish a firm grip with an object [12], [16]–[19].

While there are many differential mechanisms embodiments [20], we choose an embodiment that is likely to work within the human forearm in orthopedic surgery—namely, a rod is inserted in between the FDP tendons (see Fig. 1(c)) [13], [21]. This embodiment has several advantages when compared with, say, the pulley differential mechanism that was used to demonstrate proof of concept. The pulley system was bulky, could require artificial tendons, and may cause surrounding tissue to tear due to the pulley's moving parts. In contrast, an implantable rod has a low profile, integrates with the biological tendon network, and has no moving components. The passive implantable rod has been validated in a human cadaver study [14] (see Fig. 2). This paper's goal is to optimize the rod-based mechanism's morphology and the implantation location to improve the functional outcome of the ECRL-to-FDP tendon transfer. Specifically, we determine the variables that significantly affect the device's efficacy in producing finger differential action and joint torques. Given the nonlinear

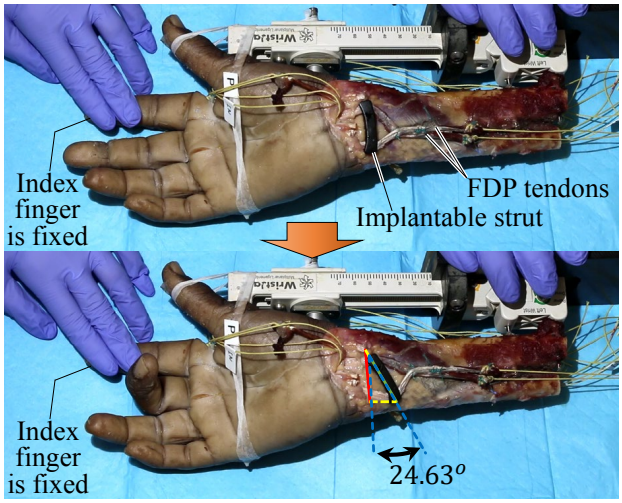

Figure 2: Depiction of the re-engineered tendon network in a human cadaver hand.

landscape for the mechanism-enabled finger biomechanics, we use genetic algorithms (GA) along with a MATLAB-based biomechanical model of the tendon network and implant to find the optimal design.

Although this work builds on the use of GAs in robot hand design [19], [22]–[25], ultrasound-guided prostate implants [26], and the beam-angle in intensity-modulated radiotherapy (IMRT) planning [27], this paper significant contributes by providing a new application domain for GAs within the biomedical engineering; namely, defining relevant biomechanical objective functions and optimizing the geometry of an orthopedic implant across multiple variables to achieve biomechanical function significantly better than hand function enabled by current surgical procedure. Furthermore, this paper focuses on only one surgical application of the implant. The differential mechanism implant can be used in all surgeries where multiple tendons are attached to a single muscle compartment to distribute movement [4]. GAs, similar to the one proposed here, can be utilized for optimizing the implant and surgical procedure as well.

II. Simulation of the Human Hand-Forearm with Implantable Mechanism

In this section, we describe a simplified biomechanical simulation model of the human forearm and hand. This model is used alongside a GA optimization procedure to find the implant design and location that produces optimal hand function (see Section IV). Grasping an object will all four fingers and requires a hierarchy of three implantable struts (see Fig. 1(c)). However, since the mechanical action of each of the three implants is similar (the implant translates and rotates to create two output-tendon movements from one input tendon movement), the model focuses on the differential action created by one implant across the two FDP tendons that drive the index and middle fingers. The work can similarly be extended across three implants arranged hierarchically, but it is beyond the scope of this paper. The parameters used in the biomechanical model are adopted from OpenSim [29] to ensure an accurate model is used in the optimization process.

Table I: Constant parameters used in the hand-forearm simulation as shown in Fig 3 (black text).

Constant Parameters	Values	Representation
d_{MCP} , d_{CT} [cm]	2.00 , 1.00 [21]	Distance between the Index and Middle finger tendons at the metacarpophalangeal (MCP) joint and carpal tunnel (CT)
k_I,k_m, k_{ECRL} [$\frac{N}{cm}$]	Force Dependent [28]	Stiffness of the Index (I) and Middle (M) finger FDP tendons and ECRL tendon
k_{θ_I}, k_{θ_M} [$\frac{Ncm}{rad}$]	10.00, 10.00 [21]	Stiffness of the Index (I) and Middle (M) finger MCP joint
L_{MCP} [cm]	10.00 [21]	Length between the MCP joint and carpal tunnel
L_{ECRL} [cm]	7.03 [21]	Length of the ECRL
L_T [cm]	24.45 [21]	Length from the MCP joint to the ECRL's insertion point
I (x,y) [cm]	(2.31, -23.70) [21]	Insertion point of the ECRL (z-axis is the normal vector off the coronal plan and O represents the Origin)

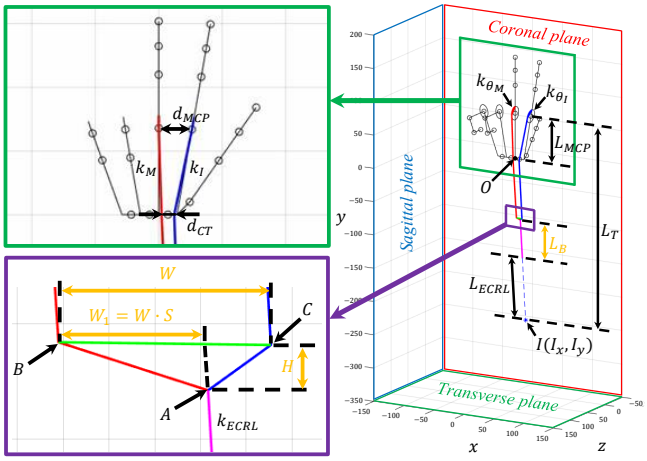

Figure 3: The kinematic representation of the human hand-forearm including the implantable mechanism. "A" is the point where the FDP tendons are sutured to the ECRL. "B" and "C" are points where the implant is connected to the FDP tendons.

It was verified that the movement and force values observed in the biomechanical simulation match with the cadaver studies we have conducted separately [14]. The optimization process can use other biomechanical models as well [30], [31].

A. Biomechanical Parameters Affecting Implant Performance

The kinematics and dynamics of the fingers' flexion (with and without the implant) are impacted by twelve constant parameters (see Table I) and four variables of interest (see Table II). Fig. 3 provides a schematic of the hand with the parameters and variables labeled (constant parameters are in black and variables are in orange). Note that the ECRL muscle's direction of pull is at angle; that is, the direction of pull is not perfectly in the proximal-distal direction. The fingers are limited to flexion and extension for simplicity. Joint rotation only occurs at the metacarpophalangeal (MCP) joint; the DIP and PIP joints are locked in an extended state for simplicity.

The four variables of interest that govern the implantable device's performance are W,H, L_B, and S. W represents the implant's width, or equivalently the base of the triangle formed between the implant and FDP tendons; H is the triangle height; L_B denotes the length between the distal end point of the ECRL and point A, shown in the purple box of Fig. 3. The implant's offset S determines the force ratio between the index and middle fingers and also whether the index and middle fingers move synchronously or sequentially. Thus, the implant can be optimized to preferentially create a two-finger pinch with, say, the index finger and thumb. If the muscle force increases after one finger has made contact, the device's rotation results in a three-finger grasp. This sequential movement enables a natural grasp. The effect of S is further discussed in section II-B2.

Table II: Implant design governing variables as shown in Fig 3 (orange text).

Variables	Representation	Initial values
W	Implant's width	1.0 cm
H	Triangle height	1.3 cm
L_B	Tendon length between ECRL distal end and Point A	11.8475 cm
S	Implant offset	0.5

B. Hand biomechanical simulation with implant incorporated

There are three important aspects to simulate the hand muscle-tendon-finger biomechanical system with the implant incorporated: (i) the system's static stability without muscle actuation or contact forces; (ii) finger movement in absence of external contact; (iii) measuring the maximum differential movement between the index and middle fingers when a finger makes contact and the muscle continues to contract. We now discuss each aspect of the developed simulation platform.

1) Static stability of biomechanical system: Before incorporating muscle actuation forces and contact between the finger and external objects, the simulation finds a statically stable configuration for the muscle-tendon-finger biomechanical system (See Appendix A for stability equations).

2) Finger movement in the absence of external contact: With the implant incorporated into the biomechanical system, the point of attachment between the ECRL and FDP tendons, point A, determines the offset S and the relative movement between the index and middle fingers in free space (absence of contact). The offset's mechanical effect is governed by the moment balance at point A. If the offset S is set to 0.5, then equal force and movement is transferred to the FDP tendons until the joint limits are reached. For simplicity, we assume in this work that the index and middle fingers are identical (stiffness and joint limits). However, the work can be extended to asymmetric biomechanics between the index and middle fingers as well.

If the offset S is set to a value other than 0.5, then different force and movement are transferred to the FDP tendons. Thus, if $S < 0.5$, more force is transferred to the middle finger. When $S > 0.5$, more force is transferred to the index finger. For example, S is set to 0.75 in Figs. 4. This setting creates the pivot point C at $0.75 \cdot W$ away from point B along the line BC. As shown in Fig. 4(a) through 4(c), more force is transferred

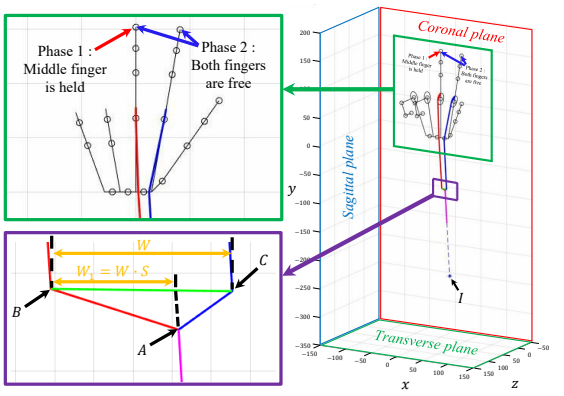

(a) The initial neutral state of the simulation for both scenarios: (1) fixed middle finger and (2) free movement.

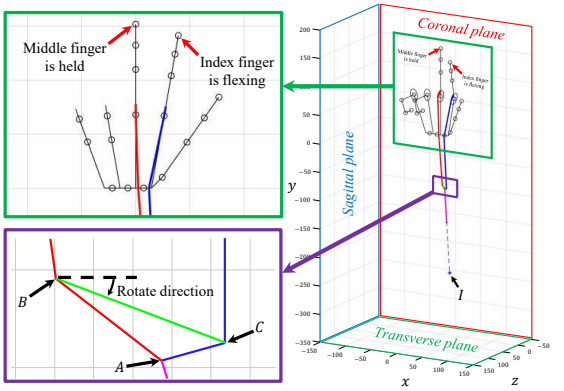

(b) The ECRL has started to contract. Fixing the middle finger forces the implant to rotate clockwise allowing the index flexure. scenario.

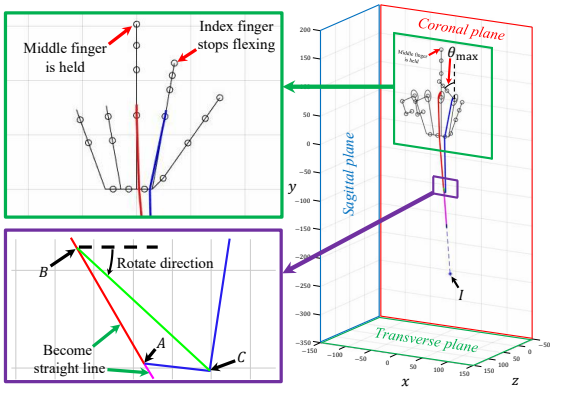

(c) ($\overline{BA}$) and ($\overline{AI}$) are collinear, signaling the simulation to terminate.

Figure 4: Depiction of the simulation's first scenario: index flexure while middle is fixed.

to the index finger. This results in the index finger flexing faster than the middle finger.

When creating movement, muscle action is simulated through control of the ECRL's muscle length (contraction by 1 mm steps). The simulation ends if the muscle reaches either its maximum force capability or maximum contraction or the finger is unable to flex further due to static balance. This step enables measuring the ECRL's maximum contraction when both fingers are flexed.

3) Differential movement between fingers with external contact: The implant's rotational freedom enables differential action between the fingers—namely, even if one finger contacts an object, the other finger can continue to flex. This is because the triangle created by the implant and tendons has three degrees of freedom—proximal/distal translation, medial/lateral translation, and rotation. In the current tendon-transfer surgery, the suture point between the ECRL tendon and FDP tendons lacks the rotational degree of freedom and can only translate proximally/distally and medially/laterally. This prevents the fingers from closing adaptively.

The fingers's biomechanics with contact is depicted in Fig. 4. Middle finger contact with the external object is simulated by locking the MCP joint. The ECRL muscle (magenta line) is contracted and static equilibrium is determined at each step. At this point, the maximum differential rotation ($\theta_{\max}$) between the index and middle finger rotation is measured.

III. Objective Functions for Evaluating Implant's Biomechanical Efficacy

The implant's biomechanical efficacy is evaluated using three physical quantities: (i) the maximum differential angle between the index and middle fingers; (ii) the maximum average torque generated at index and middle MCP joints; (iii) how close the torque ratio between the index and middle fingers is to human hand capability. Three objective functions are developed using these measures to find those implant/surgery design choices (variables W, H, S and L_B) that provide the best performance.

Objective function OF_1 measures the maximum differential angle between the index and middle fingers.For simplicity, contact is simulated by holding the middle finger fixed while the index finger is free to move. Objective function OF_2 measures the index and middle fingers' average MCP joint torque.

Objective function OF_3 balances the creation of a differential angle between the fingers and the creation of joint torques similar to human capability. This is expressed as: $OF_3 = \theta_d \cdot (1 - |\frac{\tau_{M,AVG}}{\tau_{I,AVG}} - \mu|)$. Here, θ_d is the differential angle between the middle and index fingers. $\tau_{M,AVG}$ and $\tau_{I,AVG}$ is the average torque generated by the index and middle fingers while flexing. μ represents the average MCP joint torque ratio of the index and middle in the biological human hand and is set to 1.07 [32]. Note that OF_3 does not maximize joint torques and is thus different from OF_2. While OF_3 is expressed as a simple product between the spaces represented by finger kinematics and the joint torque ratio, other relative weighting between the two spaces may also be utilized.

IV. Surgical Approach and Implant Design Optimization Using a Genetic Algorithm

The optimization procedure used in this simulation includes "Tournament selection" [33] (see Fig. 5). This process involves running several "tournaments" between designs chosen at random from the population. The winner of each tournament (the one with the best fitness) is selected for crossover.

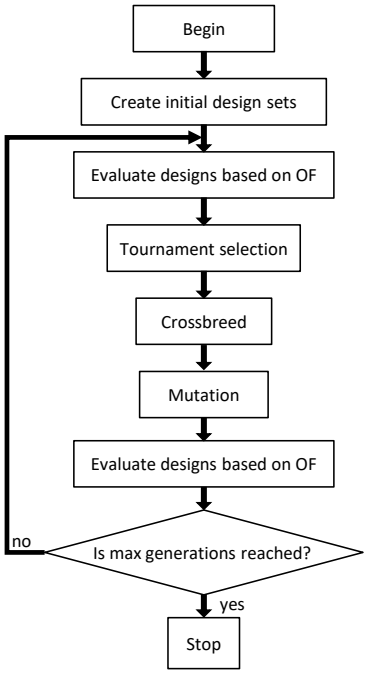

Figure 5: General method of genetic algorithm.

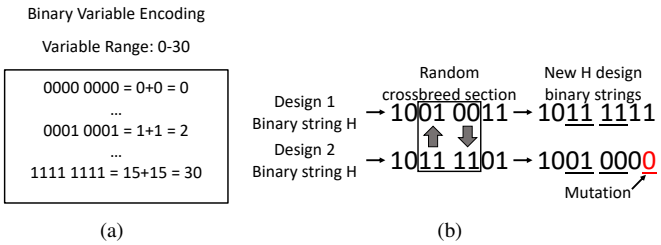

Figure 6: Depiction of (a) Variable encoding method and (b) Crossbreeding example.

The initial design set is comprised of ten implant designs. Each designs contains randomized values for the variables of interest (implant width (W), triangle height (H), offset distance (S), and the distance between the distal end point of the ECRL and point A (L_B) (orange variables in Fig. 3)).

The genetic algorithm inputs and output are represented as binary strings. The design variable value can be represented as a binary string via the boundary conditions shown in Fig. 7 (Eq. g_1 to g_8, Eq. g_9 and g_{10} keep triangle stability). Each variables range is discretized in n segments. As illustrated in Fig. 6(a), we choose 30 segments. This translates to an 8-digit long binary string (two 4-bit sets). For instance, the variable H has a range from [0.1 to 1.5] (see g_1 and g_2). After discretizing this range into $n = 30$ segments, H can take a value from [0.1 to 1.5] in intervals of 0.047. The equation to convert binary string encoded as 0100 0110 would result in a value of 0.57cm ($0100 = 4$, $0110 = 6$; $H_{\min} + (4+6) \times 0.047 = 0.57$cm). Here $H_{\min}$ is the lower boundary condition of H.

Implant designs randomly compete in a tournament style bracket using their OF. This process repeats until four designs remain. This method ensures that the best design is guaranteed to move on through the evolution process. It does not ensure

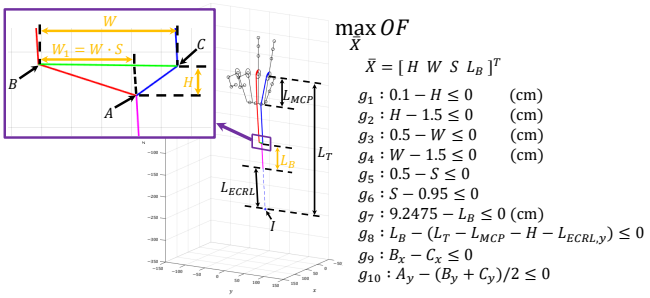

Figure 7: The optimization model and boundary conditions for each variable.

that the second, third, and fourth sets will be passed on. For instance, the second best design may compete against the third best design, effectively barring the third best design from advancing. Thus, a tournament style bracket provides a diverse solution and greater generational variability.

The four winning designs are then randomly crossbred to create six more designs. Crossbreeding is implemented by switching a random four-bit section between chromosomes from two winning implant designs (See Fig. 6(b)). Two new designs are created per crossbreed. A random four-bit section is selected, and each bit has a 5% chance of mutating (changing its value) during crossbreeding. This process is repeated for five hundred generations. The number of generations depends on the cost function landscape.

The GA is also used to optimize the current suture-based surgery. This problem is simpler than optimizing the implant-based surgery, since there is only one variable of interest; namely, the position of the suture/bifurcation point between the ECRL and FDP tendons (L_b, see Fig 3).

V. Results

We first quantify the influence of the four variables, namely, implant width W, height H, and implant offset S and the implant's location in the tendon network (L_B), on each biomechanical function OF_1, OF_2, and OF_3. We then provide the optimal solutions.

A. Influence on OF_1: Maximum Differential Angle θ_{max}

From Fig. 8(a), we notice that as W increases and H decreases for constant S and L_B, the maximum differential angle θ_{max} created at the fingers increases since the implant can pivot more. From Fig. 8(b), we notice that the maximum differential angle θ_{max} decreases marginally with L_B but does not change with S for constant H and W.

B. Influence on OF_2: Average Joint Torque τ_{avg}

Fig. 8(c) shows that the average joint torque τ_{avg} is predominantly constant as a function of H and W when L_B and S are held constant. In contrast, Fig. 8(d) shows that the average joint torque τ_{avg} is predominantly constant as a function of L_B but decreases as S deviates from symmetry, when H and W are held constant.

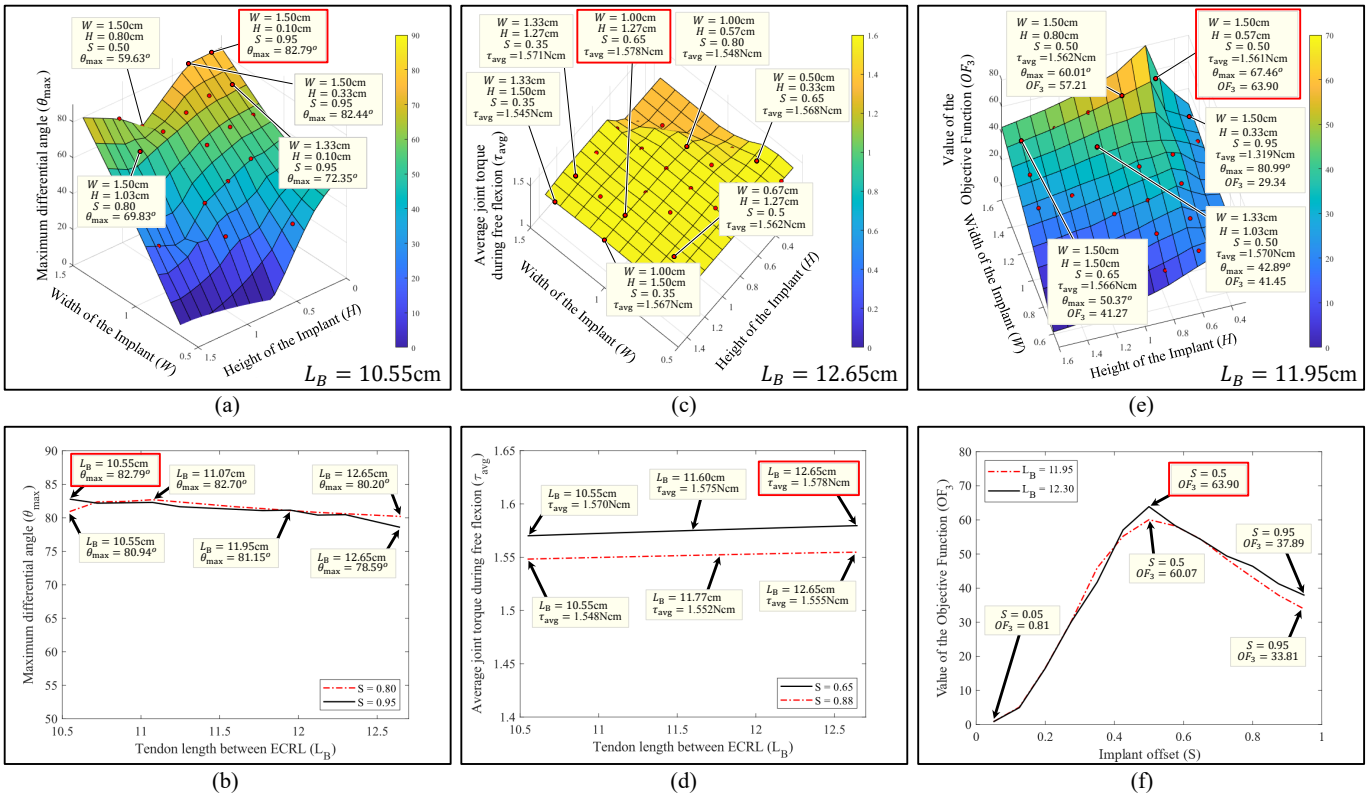

Figure 8: Landscape for (a) OF_1 when L_B is 10.55cm. The optimal variable set is boxed in red. (b) Plots the effect of L_B on θ_{max} over multiple S values. Landscape for (c) OF_2 when L_B is 12.65cm. The optimal variables set is boxed in red. (d) Plots the effect of L_B on τ_{avg} over multiple S values. Landscape for (e) OF_3 when L_B is 11.95cm. The optimal variable set is boxed in red. (f) Plots the effect of S on the value of OF_3 over multiple L_B values.

C. Influence on OF_3

Fig. 8(e) shows that the peak OF_3 value occurs when H is small, W is large, and S is close to 0.5, when L_B is held constant. Fig. 8(f) shows that peak OF_3 values occurs at $S = 0.5$ and is not affected by L_B, when H and W are held constant.

D. Optimal solutions

For the implant-based surgery, Table III shows the best function obtained from the genetic algorithm optimization using the three objective functions for the implant-based surgery. When using OF_1, maximum differential angle (82.4^o) was obtained when $W = 1.5cm$, $H = 0.1cm$, and $S = 0.80$ (see Fig 8(a)). However, the middle finger's MCP joint torque is approximately half (0.51) of index finger's MCP joint. This is significantly different from the torque ratio in a healthy human (1.07), and thus is not ideal.

The average torque τ_{AVG} produced using OF_2 and OF_3 are comparable, but the differential action produced using OF_2 is very small. Overall, OF_3 provides the best optimization result for both differential angle (67.46^o) and average torque (1.56 Ncm) of the index and middle finger's MCP joints.

For the suture-based surgery, Table IV shows the best performances obtained from the genetic algorithm optimization using the three objective functions. The maximum differential angle θ_d saturates between 5.34^o to 6^o using OF_1 and OF_3 for the suture-based surgery. This is because the suture prevents the fingers from adapting during grasping. Average torque τ_{AVG} is large for all all three objective functions.

Table III: Optimization results of the three implant cases. The bold numbers signify the result of the optimized parameter.

	OF_1	OF_2	OF_3
W [cm]	1.50	1.00	1.50
H [cm]	0.10	1.27	0.57
S	0.95	0.65	0.50
L_B [cm]	10.55	12.65	11.95
θ_d [^{o}]	**82.79**	22.98	**67.46**
τ_{AVG} [Ncm]	1.363	**1.578**	**1.561**
$\frac{\tau_{M,AVG}}{\tau_{I,AVG}}$	0.51	1.07	1.02

Overall, searching the space using OF_3 shows that the implant-based surgery provides significantly better differential action and joint torques when compared with the suture-based surgery.

VI. Discussion

A. Using genetic algorithms for optimization

This paper presents a novel method of using genetic algorithms to optimize the design of a passive orthopedic implant to improve hand function when compared with the state-of-the-art suture-based surgery. The optimizations showed that

Table IV: Optimization results of the three traditional suture cases. The bold numbers signify results of the optimized parameter.

	OF_1	OF_2	OF_3
L_B [cm]	12.83	9.31	12.32
θ_d [^{o}]	**5.34**	0.94	**5.70**
τ_{AVG} [Ncm]	1.575	**1.619**	**1.576**
$\frac{\tau_{M,AVG}}{\tau_{I,AVG}}$	1.07	1.07	1.08

the implant provides a 11X improvement in finger kinematics when compared with the suture-based surgery without compromising on the torque balance between the middle and index fingers. This implies that a patient using our implant can fully the index MCP joint while the middle finger is extended and still apply large torques.

With respect to optimization, using OF_1 and OF_2 led to significantly lopsided designs, since each objective function focused only on one of either differential angle or average torque. Specifically, in the case of implant-based surgery and when using OF_1, the maximum differential angle was 82.44^o. This was obtained when $W = 1.00cm$, $H = 1.50cm$, $L_B = 12.65cm$ and, $S = 0.5$ (see red box in Fig. 8(a)). However, the ratio of average torque between the middle finger and the index finger was 0.51 (much lower than the ratio in a healthy human of 1.07). Similarly, when using OF_2, the maximum average torque ($15.8Ncm$) of the index and middle finger's MCP joint was obtained when $W = 1.00cm$, $H = 1.50cm$, $L_B = 12.65cm$ and, $S = .5$ (see red box in Fig. 8(b)). However, this design choice only enabled 10.3^o of differential angle. Overall, OF_3 provided a balanced solution with a differential angle of 67.5^o (18.12% less than OF_1) with average torque of $15.6Ncm$ (1.03% less than OF_2. Thus, when exploring optimizations in complex processes, such as the fingers grasping objects, it is critical to consider multiple factors in the optimization function to create a solution that balances requirements.

B. Objective function landscapes

The landscapes for the three objective functions OF_1, OF_2, and OF_3 show that the biomechanical function as a function of the variables of interest is nonlinear and often non-intuitive (see Fig. 8).

Specifically, for the maximum differential angle (OF_1), a longer implant and shorter triangle enables the implant to rotate further and create larger differential action. Yet, with L_B, the relationship is more complex. Inserting the implant more proxmial (L_B small) will create longer FDP tendons. These longer tendon lead to lower torsion stiffness for the implant's rotation. This enables greater differential action. Overall, L_B does not have a significant effect on differential action for this surgery because the tendon lengths are small. L_B's impact is not fully understood until the landscape is visualized. This is particularly evident since the ECRL tendon attaches to the tendon network at an angle (not aligned along the proximal-distal line of the forearm). Furthermore, when the mechanism's effect is more complex (such as force or movement amplification in addition to differential action), implant location could play a bigger role. Finally, other vital aspects of surgical outcome, such as ergonomics/patient comfort relating to implant location could be added to the objective function [34]. Finally, the offset S does not have a significant effect on the maximum differential angle.

Considering OF_2, the average torque of the index and middle finger's MCP joints (see Fig. 8(c, d)) is not significantly affected by H, W, and L_B. This is because the force is transferred to both distal tendons being pulled equally as the ECRL contracts. However, OF_2 is only mildly affected by S, since the sum of the distal tendon forces is always equal to the muscle force.

Objective function OF_3 balances the requirement of creating large differential angle with creating joint torques similar to human ability. Such objective functions are a necessity when surgeons optimize the surgical procedure to avoid non-ideal hand function. Thus, OF_3 finds a symmetric implant geometry ($S = 0.5$) solution that creates balanced finger torques.

Importantly, the static balance equations (see Appendix A) show that this is a complex equilibrium across all four variables—a change in one variable affects the entire system. Overall, optimization using OF_3 showed that the implant enabled an 11X larger differential angle (θ_d) compared to the suture-based surgery (Implant 67.46^o, Suture 5.70^o) with only a 0.9% reduction in average torque (τ_{AVG}).

C. Comparison with cadaver experiments hand

The improved differential action enabled by the implant has also been quantified separately in other cadaver experiments [14]. Specifically, cadaver experiments showed that a rod-shaped differential mechanism, similar to the one used in this simulation, decreased the difference in fingertip force between the index and middle by 24% when compared to the the suture-based surgery. Similarly, a pulley-based differential mechanism improved the fingers' individual adaptation to the object's shape during the grasping process and reduced slip by 52% after object contact [13]. While those papers only considered a single geometry for both the implant and the surgery, the technique provided in this paper enables a thorough search across the variables in the implant-based surgery. Furthermore, the presented implant can be utilized in any procedure where the movement of multiple tendons are coupled to one muscle. These implant variations can take advantage of the presented genetic algorithm to optimize their design and provide surgical guidelines.

VII. Conclusion

This paper presents the design optimization of a novel passive implantable device used in the tendon-transfer for high median-ulnar nerve palsy. The state-of-the-art procedure results in poor grasping capability. The novel device, a strut inserted between the flexor tendons, provides significantly improved grasping capability. However, the biomechanics of the muscle, tendon, implant, and the finger function required creates a complex multi-variable problem to find the optimal device geometry and implantation location that provides best function. This paper shows that a genetic algorithms is an

effective tool to find the optimal solution across different objective functions. Additionally, the landscapes indicates that there are multiple solutions, depending on the chosen objective function. This indicates that the implant geometry and surgical procedure may be customized to every patient. Finally, this study focused on just one tendon transfer surgery. The device and the genetic algorithm used to optimize the implant can used in any surgery where multiple tendons are connected to a single muscle.

REFERENCES

[1] A. L. Douugherty *et al.*, "Battlefield extremity injuries in operation iraqi freedom," *Injury*, 2009.

[2] B. T. Corona *et al.*, "Volumetric muscle loss leads to permanent disability following extremity trauma," *J. Rehabil. Res. Dev.*, vol. 52, no. 7, pp. 785–792, 2015.

[3] A. J. .Schoenfeld *et al.*, "Spinal injuries in united states military personnel deployed to iraq and afghanistan: an epidemiological investigation involving 7877 combat casualties from 2005 to 2009," *Spine*, vol. 38, 2013.

[4] R. W. Beasley, "Tendon transfers," in *Beasley's Surgery of the Hand*, 1st ed., New York: Thieme, 2001, ch. 20, pp. 336–369.

[5] D. P. Green *et al.*, *Green's Operative Hand Surgery*, vol. 1, 2. London, UK: Elsevier Churchill Livingstone, 5th ed., 2005.

[6] A. Bookman *et al.*, *Family caregiver handbook*. Cambridge: MIT Press, 2007.

[7] P. W. Brand and A. Hollister, *Clinical mechanics of the hand*. St Louis: Mosby, 3rd ed., 1993.

[8] R. L. Lieber, "Biology and mechanics of skeletal muscle: What hand surgeons need to know when tensioning a tendon transfer," *J. Hand Surg.*, 2008.

[9] W. P. Cooney *et al.*, "Opposition of the thumb: An anatomic and biomechanical study of tendon transfers," *J. Hand Surg.*, vol. 9, no. 6, pp. 777–786, 1984.

[10] D. M. Sammer and K. C. Chung, "Tendon transfers: Part I. principles of transfer and transfers for radial nerve palsy," *Plast. Reconstr. Surg.*, vol. 123, pp. 169e–177e, May 2009.

[11] D. M. Sammer and K. C. Chung, "Tendon transfers: Part II. Transfers for ulnar nerve palsy and median nerve palsy," *Plast. Reconstr. Surg.*, vol. 124, no. 3, pp. 212e–221e, 2009.

[12] A. M. Dollar and R. D. Howe, "The highly adaptive sdm hand: Design and performance evaluation," *Int. J. Robot*, vol. 29, no. 5, pp. 585–597, 2010.

[13] K. Mardula *et al.*, "Implanted passive engineering mechanism improves hand function after tendon transfer surgery: A cadaver-based study," *HAND*, vol. 10, no. 1, pp. 116–122, 2015.

[14] S. C. Raja *et al.*, "Novel passive implanted differrential mechanism improves grasp function after tendon transfer surgery." presented at the 12th Tetrahand World Congress, Nottwil, Switzerland, Aug. 28-31, 2018.

[15] J. Montgomery *et al.*, "New tendon-transfer surgery for ulnar-median nerve palsy using embedded adaptive engineering mechanisms," in *Proc. CMBBE*, April 2013.

[16] L. Birglen *et al.*, *Underactuated robotic hands*. New York: Springer, 2007.

[17] R. R. Ma *et al.*, "A modular, open-source 3d printed underactuated hand," in *Proc. ICRA*, pp. 2737–2743, May 2013.

[18] W. S. You *et al.*, "Design of backdrivable soft robotic finger mechanism," in *Proc. URAI*, pp. 343–344, December 2015.

[19] W. S. You *et al.*, "Kinematic design optimization for anthropomorphic robot hand based on interactivity of fingers," *Intell. Serv. Robot.*, vol. 12, pp. 197—208, 2019.

[20] R. Balasubramanian *et al.*, "Implanted passive engineered mechanisms and methods for their use and manufacture," U.S. Patent 10 595 984, Mar 24, 2020.

[21] T. Homayouni *et al.*, "Modeling implantable passive mechanisms for modifying the transmission of forces and movements between muscle and tendons," *IEEE Trans. Biomed. Eng.*, vol. 62, no. 9, pp. 2208–2214, 2015.

[22] H. Wang *et al.*, "An anthropomorphic design guideline for the thumb of the dexterous hand," in *Proc. ICMA*, pp. 777–782, August 2012.

[23] J. M. Inouye and F. J. Valero-Cuevas, "Anthropomorphic tendon-driven robotic hands can exceed human grasping capabilities following optimization," *Int. J. Robot*, vol. 33, no. 5, pp. 694–705, 2014.

[24] W. S. You *et al.*, "Kinematic design optimization of improved branched tendon mechanism using genetic algorithm," in *Proc. URAI*, pp. 771–776, July 2017.

[25] W. S. You *et al.*, "Kinematic design optimization of anthropomorphic robot hand using a new performance index," in *Proc. URAI*, pp. 20–25, July 2017.

[26] Y. Yu and M. C. Schell, "A genetic algorithm for optimization prostate implants," *Med. Phys.*, vol. 23, no. 12, pp. 2085—2091, 1996.

[27] Y. Li and J. Lei, "A feasible solution to the beam-angle-optimization problem in radiotherapy planning with a dna-based genetic algorithm," *IEEE Trans. Biomed. Eng.*, vol. 57, no. 3, pp. 499–508, 2010.

[28] C. N. Maganaris and J. P. Paul, "In vivo human tendon mechanical properties," *J. Physiol.*, vol. 521, no. 1, pp. 307–313, 1999.

[29] S. L. Delp, , *et al.*, "OpenSim: Open-source software to create and analyze dynamic simulations of movement," *IEEE Trans Biomed. Engineering*, 2007.

[30] LifeModeler, "LifeModeler Professional Biomechanics Software." http://www.lifemodeler.com/.

[31] Anybody, "Anybody Professional Biomechanics Software." https://www.anybodytech.com/software/.

[32] A. B. Swanson *et al.*, "The strength of the hand," *Bull. Prosthet. Res.*, vol. 10, no. 14, pp. 145–153, 1970.

[33] B. Miller and D. Goldberg, "Genetic algorithms, tournament selection, and the effects of noise," *Complex Syst.*, vol. 9, pp. 193–212, 1995.

[34] J. Haglin, A. Eltorai, and J. A. Gil, "Patient-specific orthopaedic implants," *Orthopaedic Surgery*, vol. 8, no. 4, pp. 417–424, 2014.

APPENDIX A: STATIC STABILITY EQUATIONS

These following equations represent the biomechanical system's (as shown in Fig. 3) static stability. Equations (1) - (3) are static balance equations for the tendon network. Equation (1) governs the the connection point between the ECRL and FDP (Point A in Fig. 3). Equations (2) and (3) govern the index and middle MCP joints. Equations (4) and (5) (see (6) and (7) for constituent parts) are the force and moment static balance equations for the implantable device. Static stability is reached when (1) to (5) are equal to zero.

$$F_{\text{Apex}} = k_{ECRL} * L_B[-c_{\theta_a}; -s_{\theta_a}] + k_{AtoB} * L_{AtoB}[c_{\theta_b}; s_{\theta_b}] + k_{AtoC} * L_{AtoC}[c_{\theta_b-\theta_x}; s_{\theta_b-\theta_x}] \tag{1}$$

$$F_{MCP_M} = \frac{L_{M_{MCP}}}{R_{MCP}} * k_{\theta_M} - (L_{BtoM_{MCP}} - L_{M_{MCP}} * R_{MCP}) * k_M \tag{2}$$

$$F_{MCP_I} = \frac{L_{I_{MCP}}}{R_{MCP}} * k_{\theta_I} - (L_{CtoI_{MCP}} - L_{I_{MCP}} * R_{MCP}) * k_I \tag{3}$$

$$M_{\text{Implant}} = k_I * (L_{CtoI_{MCP}} - L_{I_{MCP}} * R_{MCP})[c_{\theta_2}; s_{\theta_2}] \times (C - B) + k_{AtoC} * L_{AtoC}[c_{\theta_W}; s_{\theta_W}] \times (C - B) \tag{4}$$

$$F_{\text{Implant}} = F_{\text{Implant}_L} + F_{\text{Implant}_R} \tag{5}$$

$$F_{\text{Implant}_L} = k_M * (L_{BtoMCP} - L_{M_{MCP}} * R_{MCP})[c_{\theta_1}; s_{\theta_1}] + k_{AtoB} * L_{AtoB}[c_{\theta_Z}; s_{\theta_Z}] \tag{6}$$

$$F_{\text{Implant}_R} = k_I * (L_{CtoMCP} - L_{I_{MCP}} * R_{MCP})[c_{\theta_2}; s_{\theta_2}] + k_{AtoC} * L_{AtoC}[c_{\theta_W}; s_{\theta_W}] \tag{7}$$

.

Table V: Static stability variables used in the above equations. See Fig. 3 for a visual representation.

Variables	Representation
Tendon and Joint Stiffness	
k_I,k_m, k_{ECRL} $[N/cm]$	Index (I) and Middle (M) finger FDP tendons and ECRL tendon stiffness
k_{AtoB},k_{AtoC} $[N/cm]$	Implant attachment points (B and C) to triangle apex (Point A) tendon stiffness
k_{θ_I}, k_{θ_I} $[Ncm/rad]$	Index (I) and Middle (M) finger MCP joint stiffness
Tendon and Joint Lengths	
L_B [cm]	Tendon length between the ECRL muscle and triangle apex
L_{AtoB}, $L_{AtoC}[cm]$	Tendon length between implant attachment points (B and C) to triangle apex (Point A)
$L_{M_{MCP}}$, $L_{I_{MCP}}$ [Rad]	Tendon length over Middle (M) and Index (I) MCP joints
$L_{BtoM_{MCP}}$, $L_{CtoI_{MCP}}[cm]$	Tendon length between implant attachment points (B and C) and MCP joints
R_{MCP} [cm]	MCP radius
Angles	
θ_a	Angle between the ECRL muscle and the x-axis (at point I)
θ_b	Angle between points A and B and the x-axis (at point A)
θ_x	Apex angle of ABC triangle
θ_w	Angle between point A, point C, and the x-axis (at point C)
θ_z	Angle between point A, point C, and the x-axis (at point B)
θ_1	Angle of Index FDP tendon, point C, and the x-axis (at point B)
θ_2	Angle of Middle FDP tendon, point B, and the x-axis (at point C)
Additional Variables	
c, s	cosine and sine